Steady downslope movement on the western flank of Arenal volcano, Costa Rica

S. K. Ebmeier

COMET+, Department of Earth Sciences, University of Oxford, South Parks Road, Oxford OX1 3AN, UK (susannae@earth.ox.ac.uk)

J. Biggs

COMET+, Department of Earth Sciences, University of Oxford, South Parks Road, Oxford OX1 3AN, UK

Now at Department of Earth Sciences, University of Bristol, Queen's Road, Bristol BS8 1RJ, UK

T. A. Mather

COMET+, Department of Earth Sciences, University of Oxford, South Parks Road, Oxford OX1 3AN, UK

G. Wadge

COMET+, ESSC, University of Reading, Reading RG6 6AL, UK

F. Amelung

RSMAS, University of Miami, 4600 Rickenbacker Causeway, Miami, Florida 33149, USA

[1] The edifice of a volcano is a unique deformational environment, dependent not just on active volcanic processes but also on its composition, structure, and morphology. We measured the deformation of Volcán Arenal, Costa Rica, using interferograms constructed from both ALOS and RadarSat data between 2005 and 2009. The volcano's western flanks are moving downslope at an angle of ~55° below the horizontal plane and a consistent rate of at least ~7 cm/yr. We use the pattern, rate, and direction of motion to test several hypotheses for its origin. Our favored explanation is creep along a shallow sliding plane, most likely the interface between deposits postdating the 1968 lateral blast eruption and the older lavas and paleosoils beneath. Our measurement of slope movement adds to a small set of rate measurements for gravity-driven deformation at volcanoes and is distinctive in both its relatively high rate and shallow origin. Observation of deformation at Arenal contributes both to the assessment of particular hazards around Arenal itself and, more generally, to the study of the stability of young stratovolcanoes.

1. Introduction

[2] The deformation of a volcano is caused by both volcanic activity and mechanical processes associated with the building and settling of an edifice. Volcano deformation is most commonly measured with the aim of illuminating magmatic processes. Deformation caused by the emplacement of magma, for example, can be used to obtain an estimate of the depth, volume and, to some extent, the shape of a magma chamber or dike. For some volcanoes, monitoring deformation at high temporal resolution may also provide advance warning of eruptions or changes in level of activity. However, measurements of deformation also capture surface processes, such as the subsidence of fresh eruptive products [e.g., *Stevens et al.*, 2001a] and spreading of the edifice [e.g., *Lundgren et al.*, 2004]. Volcanoes are built of poorly consolidated rock at rates greatly exceeding those of erosion, making them inherently unstable. At many active and dormant volcanoes, edifice instabilities present a significant hazard to surrounding populations, from localized rockfalls to massive sector collapses [*Ward and Day*, 2003]. The dangers associated with an unstable edifice are most extreme where the removal of an overburden could cause rapid decompression of a magma body and trigger an eruption. The best chance of identifying regions of instability on a volcano comes from understanding and monitoring the deformation of its edifice.

[3] Volcán Arenal is Costa Rica's most active volcano, and has been almost continuously erupting for ~40 years. Arenal was dormant for several centuries before its reactivation in July 1968 [*Minakami and Utibori*, 1969], when a lateral blast and subsequent vulcanian eruption killed 78 people and destroyed two nearby villages. An area of around 15 km^2 was severely damaged during 3 days of blast eruptions and a further 230 km^2 experienced significant ash fall [*Alvarado et al.*, 2006]. The eruption blast opened up a radial fissure running west from the summit, feeding three explosion craters (labeled A, B, and C in Figures 1b and 1c). Crater D, at the then summit of the volcano, has remained inactive through the current phase of activity. Since this initial eruption, activity at Arenal has shifted through several phases, with a general trend of decreasing effusion rate (2 m^3 s^{-1} in 1968 to 0.086 m^3 s^{-1} between 2000 and 2004 [*Wadge et al.*, 2006]). In 1973, during a brief pause in activity, lava effusion shifted from the lowest of the new explosion craters (A) to the highest (C), which has been active ever since. Today, activity at Arenal is dominated by occasional, short lava flows and intermittent low-level explosions, with only 4–6% of Arenal's total output being pyroclastic flows [*Wadge et al.*, 2006] which currently present the biggest hazard to the population around Arenal.

[4] Today at least 7000 people live within a 6 km radius of Arenal, mostly in the town of La Fortuna, where most of the population is to some extent dependent on volcano and hot spring related tourism for their livelihood. Lake Arenal, which extends to within 4 km of Arenal's western flank, was created in 1979 by the building of the Sangregado Dam, which supplies a high proportion of Costa Rica's hydroelectricity (Figure 1).

[5] We use interferometric data to measure the deformation of Arenal's edifice over 4 years between late 2005 and mid-2009. The rate of motion was found from time series analysis, and components of motion were resolved from imagery with different look angles. Different scenarios for the origin of the deformation of Arenal's western flanks are then considered and tested against information deduced from analysis of the results from interferometry and existing structural, geophysical, volcanological and petrological information.

2. InSAR Data

[6] Interferometric Synthetic Aperture Radar (InSAR) uses the change in the phase component of returned radiation from time separated radar acquisitions to measure small displacements of the Earth's surface. It has been applied to a broad range of volcanic environments [e.g., *Zebker et al.*, 2000] and measures ground deformation with a broad spatial coverage and centimetric precision. Change in phase is the sum of phase shifts caused by changes in satellite position and associated perspective effect on topography, variations in atmospheric composition, the scattering properties of the ground surface and deformation of the ground.

[7] Interferograms were constructed from two sets of satellite data: ALOS (mid-2007 to 2009) and Radarsat (late 2005–2008). Interferometry is only successful where surface scatterer properties are changing slowly enough for phase to remain coherent. Decay in coherence (decorrelation) depends on radar wavelength (23 cm for ALOS and 5.6 cm for Radarsat). A significant number of interferograms produced; ~75% of the Radarsat and ~30% of the available ALOS were incoherent over Arenal and were discarded. 40 interferograms that were phase
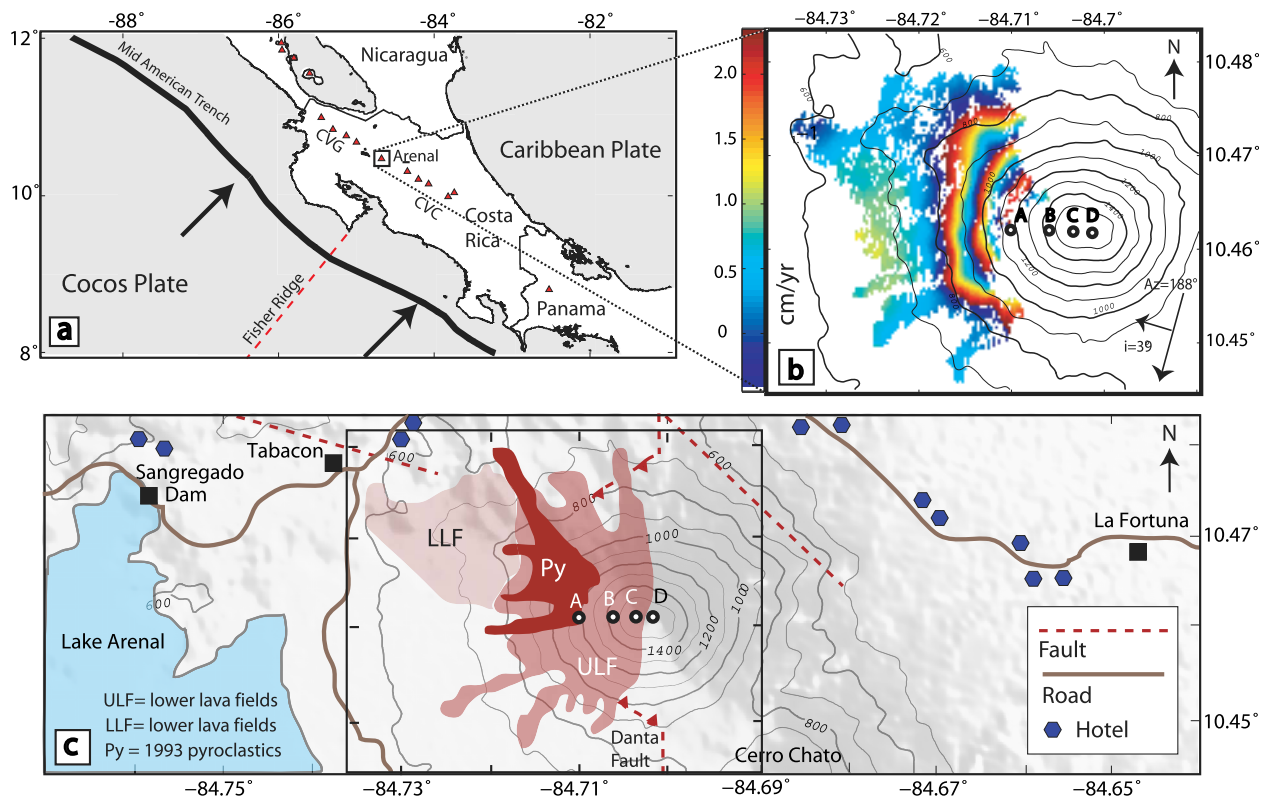
Figure 1. (a) Map showing the location of volcanoes in Costa Rica. (b) Average LOS deformation rate in cm/yr for descending Radarsat interferograms 2005–2008. Figure 1b is wrapped so that one complete transition through the color scale represents 2.56 cm deformation. (c) Schematic map showing the extent of the post-1968 lavas [after *Wadge et al.*, 2006; *Alvarado et al.*, 2006] and the locations of towns, hotels, and significant infrastructure. Craters A–D are represented by open circles. LLF, lower lava fields (1968–1973); ULF, upper lava fields (1974–2005). Pyroclastic flow (Py) deposits are from 1993. Active faults (younger than 4 ka) are marked by red dashed lines, including the Danta fault. *Alvarado et al.* [2006] infer the presence and location of the thrust fault shown here from pre-1968 aerial photography. The box used for Figure 1b and in Figures 2–4 is outlined in Figure 1c.

coherent over at least parts of the volcano's edifice remained, and were used in analysis.

[8] Interferograms were processed using the Repeat Orbit Processing software (ROI_PAC) developed at Caltech/JPL [*Rosen et al.*, 2004]. Topographic corrections were applied using the 90m digital elevation model from NASA's Shuttle Radar Topography Mission, interpolated and resampled to a spacing of 30m [*Rosen et al.*, 2004]. For each interferogram the phase was converted to displacement in centimeters relative to a coherent reference pixel. Unwrapping was carried out manually by correcting fringes individually in the wrapped interferograms using an interactive MATLAB script for ALOS and using the snaphu algorithm for Radarsat [*Chen and Zebker*, 2002]. Linear ramps in the phase data of an interferogram can be caused by inaccuracies in the satellite orbital positions. Where the far field was sufficiently

coherent, orbital ramps were sampled, modeled and subtracted from the interferogram. Data were discarded where significant ramps could not be removed.

[9] The interferograms show a consistent pattern of fringes on Arenal's western flanks for the whole time between December 2005 and April 2009 (Figure 2). All of the longer-period interferograms (Figures 2a, 2c, 2e, and 2g) show a remarkably similar, sharp-cornered subsidence signal, increasing in rate toward the volcano summit. Short time period interferograms (Figures 2b, 2d, 2f, and 2h) exhibit greater variation in signal shape, with peak subsidence appearing on different parts of the volcano on different dates, indicative of a block-like motion. This shows that although the average pattern of deformation is relatively constant between 2006 and 2009, the instantaneous rate of motion
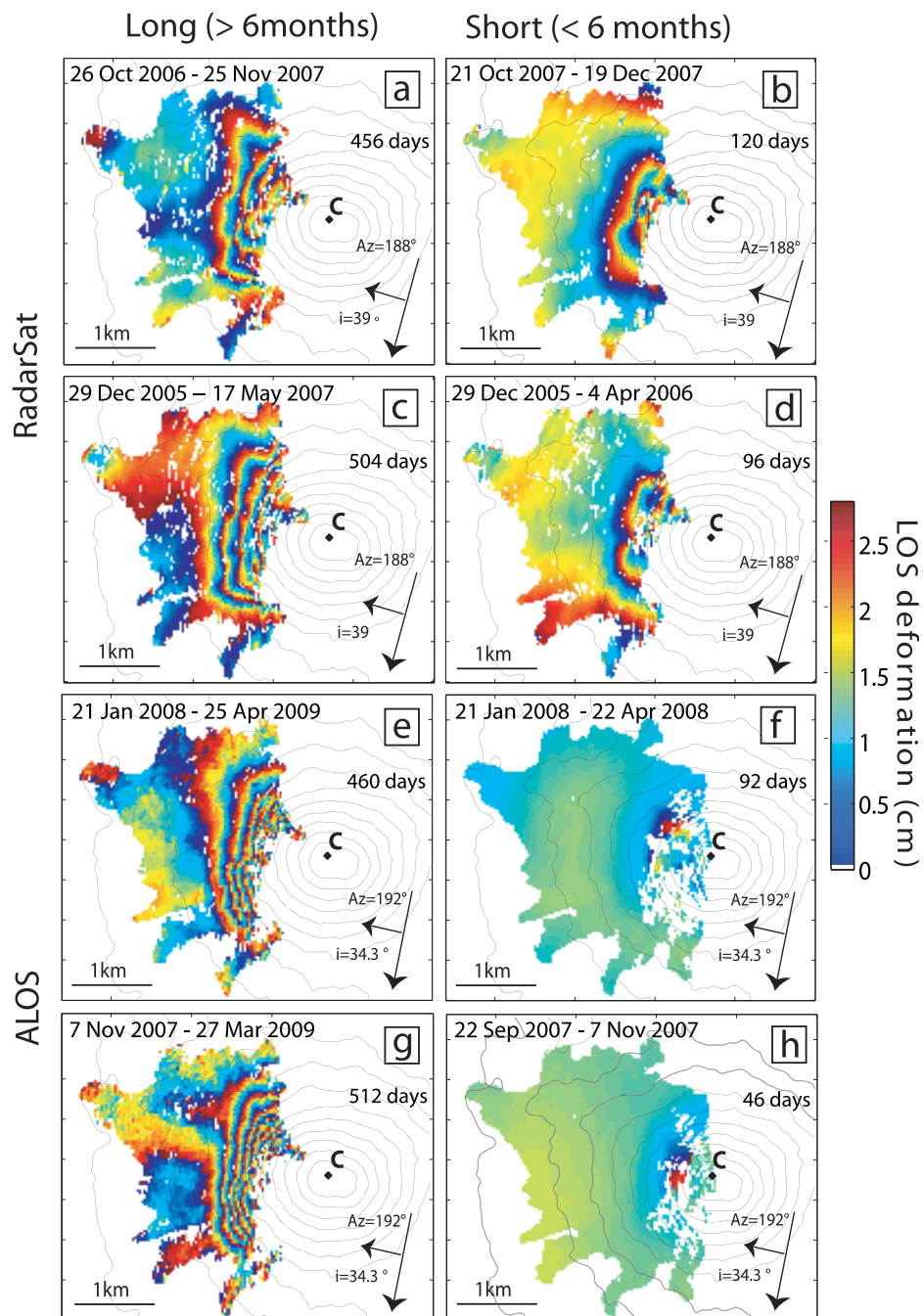
Figure 2. Sample (a–d) Radarsat and (e–h) ALOS interferograms showing typical deformation signals for time periods greater than 6 months (Figures 2a, 2c, 2e, and 2g) and less than 6 months (Figures 2b, 2d, 2f, and 2h). All interferograms are wrapped to C band and projected over topographic contours as for Figure 1b. The active summit crater is marked C, as in Figure 1. Azimuth (Az) and incidence angles (i) are indicated for each interferogram.

varied with space and time across Arenal's edifice (see section 2.4 and Figure 4).

2.1. Patterns of Coherence

[10] Interferometry is phase decorrelated where the baseline separation of the satellite between acquisitions is high or slopes are too steep (geometric decorrelation) and surface scattering properties change quickly (temporal decorrelation). Temporal decorrelation is typically associated with dense, fast growing vegetation, unstable slopes and the eruption, emplacement and settling of fresh volcanic products.

All of these factors have a significant effect at Arenal. Coherence is therefore limited to parts of the western slopes of the volcano, roughly defined by the edges of the post-1968 lavas, but stopping short of the summit (Figure 2).

[11] The response of L (λ = 23 cm) and C band (λ = 5.6 cm) radar to vegetation is markedly different, with L band having been demonstrated to have better coherence in highly vegetated regions than C band [e.g., *Fournier et al.*, 2010]. This is illustrated by the difference between Radarsat (C band) and ALOS (L band) interferograms of Arenal (Figure 2). Variations in coherence are associated with changes in the lava surface stability. The best coherence is on young lava fields, which generally have exceptional scatter stability [*Lu and Freymueller*, 1998]. In all but the shortest time period interferograms (Figures 2f and 2h), coherence breaks down above an elevation of about 1100 m. Below this height the surface is grown through with low-lying vegetation and is sufficiently stable for drainage channels of height ~10–30 m to be established. Above this height, slopes are much less stable, with no drainage channels and semi-continuous rockfalls as a consequence of the high rate of break up of steep lava fronts near the summit. However, a few short-period ALOS interferograms (Figures 2f and 2h) show that subsidence does not extend all the way up to crater C, but reaches its peak value between 1200–1440 m elevation.

[12] The lack of coherence on Arenal's eastern slopes is attributed to a combination of denser, more mature vegetation right up to the summit and loose, rockfall prone material. Furthermore, the eastern side of the volcano is roughly perpendicular to the radar look direction for descending acquisitions, (which constitute 92% of interferograms used) and is therefore foreshortened in radar geometry. We do not extrapolate our observations onto the eastern flank because none of the observed fringes, the volcano structure or young flows are radially symmetric. The signal we observe is limited to young (<40 years) lava flows, while material east of the summit is predominantly older and cannot be assumed to be deforming in the same way.

2.2. Topographic Artifacts

[13] A concern in the interpretation of the Arenal data set was the possibility that any apparent deformation signal could be an artifact caused by the difference between the DEM used in processing and actual topography. This could be either because of uncertainty in the SRTM data used to construct the DEM, or because the volcano's surface has changed significantly since 2000, when the SRTM data were acquired [*Rosen et al.*, 2001].

[14] The first possibility is relatively easy to discount, since the uncertainty in SRTM data in Costa Rica is expected to be ~5–7 m [*Rodriguez et al.*, 2006]. For the Arenal interferograms (Table S2 in the auxiliary material), the greatest risk of DEM errors contaminating any deformation signal will be for those C band interferograms of longest baseline separation, but the altitude of ambiguity for even the longest of these is still many times the expected error in the SRTM data.

[15] The second option, of there being significant topographic change since the DEM data were collected, was tested by examining the relationship between perpendicular baseline separation and magnitude of apparent deformation. An artifact in phase change caused by a DEM error is expected to be proportional to baseline separation [e.g., *Hooper et al.*, 2004], so the lack of correlation between the two properties in the Arenal data (Figure S1 in the auxiliary material) suggests that the phase shift at Arenal represents a genuine ground movement.[1] This is reasonable as the lava emplaced since 2000 has not extended beyond the incoherent zone around Arenal's summit. Between 2000 and 2004 a maximum thickness of around 40 m of lava was emplaced, but never extended any farther downslope than crater A [*Wadge et al.*, 2006]. Between 2005 and 2010 lava effusion rates have been even lower. We conclude that the SRTM data are an accurate reflection of Arenal's current topography in coherent areas, and that the phase signal represents real deformation and not a DEM error.

[16] Artifacts caused by topographically correlated variations in water vapor [*Wadge et al.*, 2002] are identifiable from their association with particular acquisition dates and their tendency to change sign depending on whether the image is used as the master or slave. The fact that apparent deformation is consistent in sign and approximate rate in all interferograms allows the possibility of a significant stratified water vapor effect to be disregarded.

2.3. Components of Motion

[17] InSAR measures displacement along a single line of sight. Multiple measurements from different look angles can be combined to resolve this into a full 3-D deformation field [e.g., *Wright et al.*,

2004]. In practice, interferograms can be produced from SAR data from ascending and descending orbits, providing only 2 independent constraints on a three-dimensional problem. Resolving components of motion therefore requires an external source of information or an assumption [e.g., *Fialko et al.*, 2001]. The assumption was therefore made that N-S motion was negligible, allowing us to resolve the volcano's deformation field into a 2-D plane with axes running vertically and E-W [e.g., *Biggs et al.*, 2009].

[18] This assumption is reasonable since ascending and descending satellites look from close to due east and west, respectively, and will therefore only capture a minor component of N-S motion (the N component of the line of sight unit vector is −0.1). A pair of ascending and descending interferograms (Figures 3a and 3b) were converted to rate before the inversion, since their time spans were not coincident. The lack of deformation signal in the ascending interferogram suggest that their LOS vertical and horizontal components of motion cancel each other out and are therefore likely to be of similar magnitude. Vertical and east-west components of motion were then resolved pixel by pixel from the LOS displacements of the two interferograms, and used to calculate the total magnitude and angle of motion. The limited number of ascending interferograms mean that angle of motion could only be found for September 2007 to January 2008. The LOS displacement rates, patterns and magnitude of the interferograms used in the inversion were typical of the rest of the data set. For the descending data this meant that the rate fell within the error bounds of the mean value found from a time series constructed from the complete data set (section 2.4). This allows us some confidence that the components of motion calculated are representative.

[19] The angle of deformation obtained from the inversion of different lines of sight allows us to refine our picture of slope movement at Arenal. The downward and westward components of motion are of similar magnitude, with the upper slopes moving at angle of ~50° below the horizontal. There is a sharp boundary (Figure 3) between this shallow downward and westward motion of around 12 cm/yr and the steeper, lower-magnitude motion at the base of Arenal's slopes. This change in angle and rate of motion is level with the zone where the volcano slopes becomes shallower, but is still a notable boundary if the angle of motion is normalized for the slope gradient, as in Figure 3.

2.4. Time Series

[20] The temporal distribution of interferograms over Arenal is controlled by the distribution of ALOS and Radarsat acquisitions, baseline separations and the rates of decorrelation at different radar wavelengths. The interferograms used in the analysis at Arenal (Table S1 in the auxiliary material) are therefore unevenly distributed, making any temporal variations in subsidence rate very difficult to detect directly from the interferograms.

[21] A time series can generally be constructed for a network of interferograms by using a linear least squares inversion of the displacements for each interferogram to find the incremental displacements between acquisition dates [*Berardino et al.*, 2002; *Schmidt and Bürgmann*, 2003]. As the number of acquisition dates will always be one greater than the number of intervals between them, the displacements must be solved relative to a reference time where it is assumed that there is no deformation, in this case the first date. Inversion was carried out using a generalized inverse (the Moore-Penrose pseudoinverse) matrix, found from singular value decomposition. Unrealistic discontinuities are avoided by fitting the minimum constraint to velocity over a time interval rather than displacement [*Berardino et al.*, 2002]. Interferograms over Arenal were constructed using four different satellite tracks and therefore make up four independent groups. The three interferograms from ALOS ascending data are of poor coherence and were not used in the time series construction, leaving three

Figure 3.   (a) Ascending ALOS and (b) descending Radarsat interferograms used to find best fit components of motion in two dimensions. (c) East-west and (d) vertical components of motion resolved using the assumption that north-south motion was negligible. Negative rates represent westward and downward motion. The dotted line represents the trace of the profiles shown in Figures 3e and 3f. (e) The total magnitude and angle of motion shown as vectors on a transect through Arenal's summit, so that the arrow length is proportional to the rate. Due to limited coherence, the average value of an area at the western edge of the lava fields was used as a reference point assumed to experience no deformation. (f) Cross section of Arenal's post-1968 deposits as estimated using the lava isopach maps constructed by *Wadge et al.* [2006]. The boundary between pre-1973 (from crater A) and post-1973 lavas is estimated from the profiles for which topographic data were available.
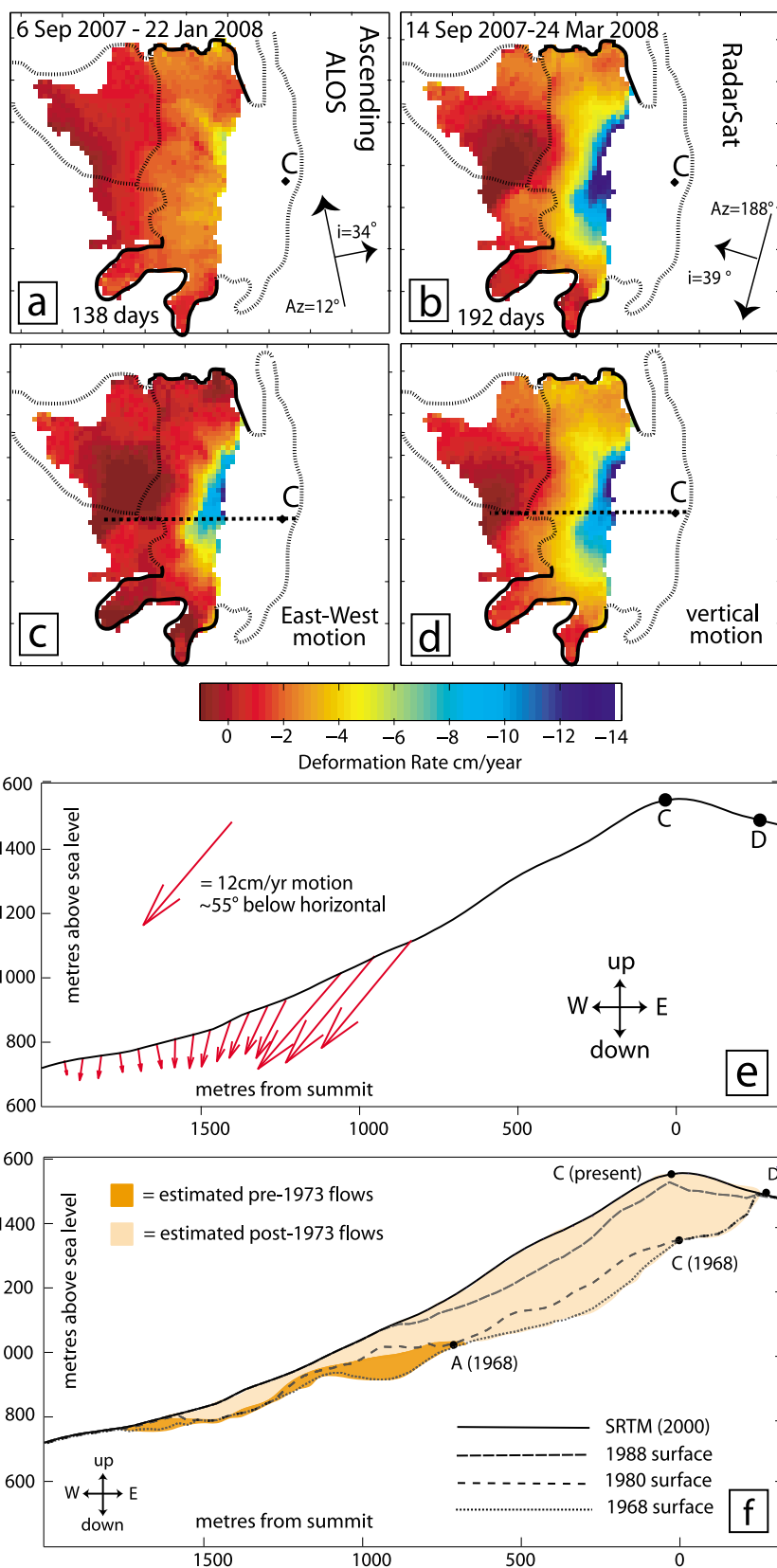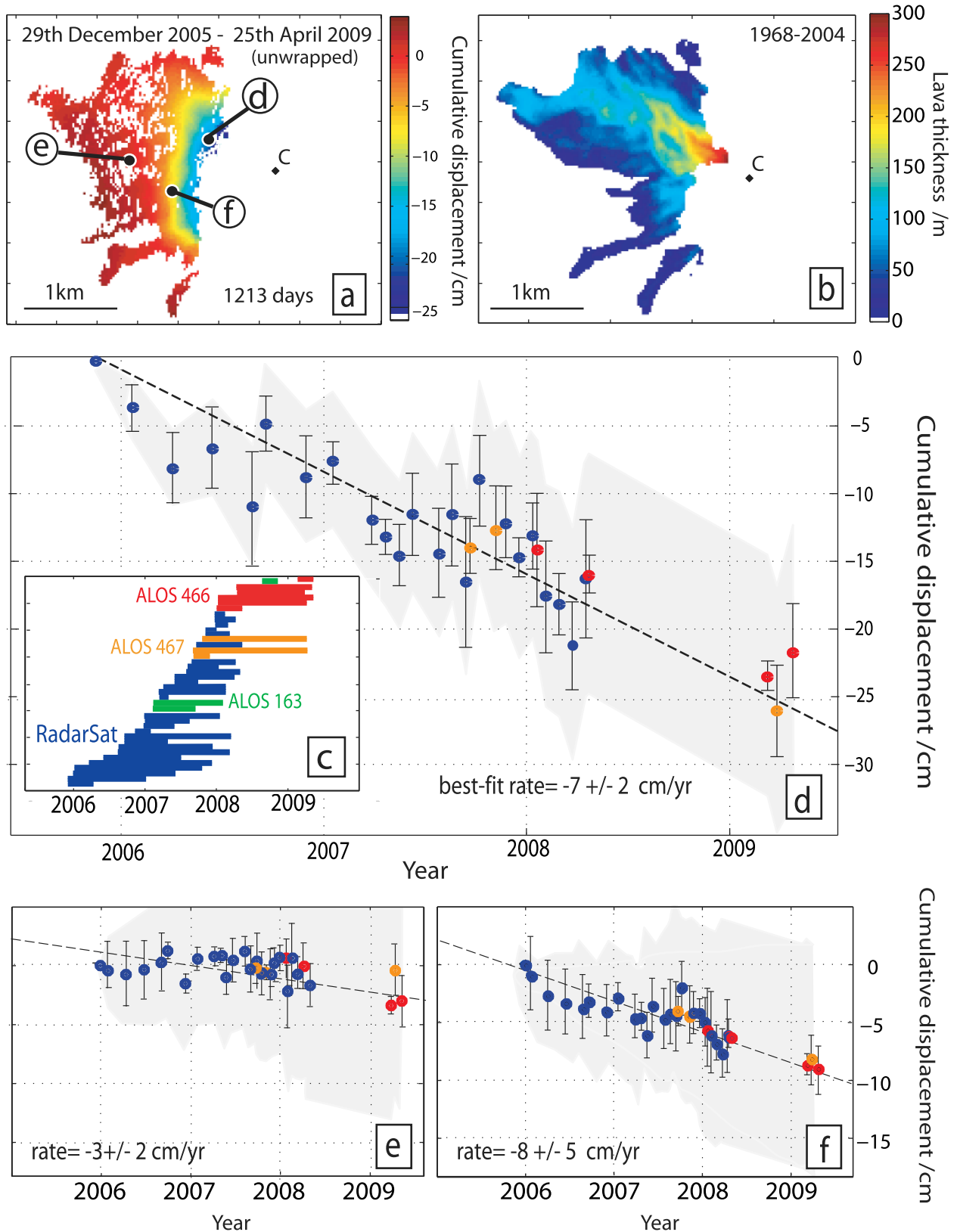
Figure 3

Figure 4

independent groups of dates (Table S1 in the auxiliary material and Figure 4c).

[22] We created links between isolated groups of acquisitions from different tracks by assuming that the displacement between acquisition dates less than 8 days apart was negligible. For a typical deformation rate (6 cm/yr), 8 days of motion would produce at most a millimeter of displacement. This was seen to improve the reliability of our velocity solutions in tests using synthetic data.

[23] We use a Monte Carlo inversion to estimate errors on the time series, which are likely to include random atmospheric noise in the original interferograms, topographic correlations in water vapor and orbital ramps. The Arenal lava fields make up the only coherent part of most of the interferograms used, so the last two sources cannot be entirely eliminated by inspection of the far field. We simulate atmospheric noise by adding an element of normally distributed random noise to every pixel in every interferogram. The noise had a mean amplitude of 1cm [e.g., *Pritchard and Simons*, 2004], but the effects of spatial correlation were neglected. We repeated the procedure 100 times to find the distribution of uncertainty in the resulting velocities. This uncertainty reflects the strength of links to the rest of the network for each acquisition date and is not evenly distributed across the acquisition dates. The errors between adjacent acquisitions are typically 1–4 cm and cumulative errors on rate are 2–5 cm/yr.

[24] Time series from Arenal show a steady average rate of motion for the whole period of 2005–2009, with best fit rates of between ~6 and 8 cm/yr found from least squares inversion. In Figure 4d we show a representative time series from the center of the western flank (location marked in Figure 4a). In a few locations there are sharp changes in rate of motion (e.g., the start of 2008 (Figure 4f)), suggesting that parts of Arenal's slopes may be moving as discrete blocks. However, these variations lie within the bounds of uncertainty, so it is not possible to determine conclusively whether motion is spatially and temporally discontinuous or uniform and constant.

2.5. Comparison of InSAR Results With Electronic Distance Meter Measurements

[25] The magnitude and direction of movement observed with InSAR is supported by electronic distance meter measurements made by OVSICORI-UNA since 2008 on 5 locations on Arenal's western flank. These show a shortening of the distance between a control station at the base of the volcano and 4 reflectors at different distances due east up the flanks. The highest of these two reflectors (~890 m and ~840 m asl) allow measurement of a contraction rate of ~6 cm/yr in the E-W direction, a value that corresponds well with those found from the InSAR components of motion at an equivalent height. The limits of this contraction also match well to the remote sensing data, as reflectors below about 780 m asl do not appear to be getting closer to the reference station. This east-west contraction has been interpreted to be a consequence of spreading caused by substrate relaxation [*Alvarado et al.*, 2010; R. van der Laat, personal communication, 2010].

3. Discussion

[26] A range of processes associated both with magmatic activity or structural instabilities can cause deformation of a volcano's edifice. At Arenal, conceivable origins for a subsidence signal include (1) magmatic deflation (e.g., Okmok [*Lu et al.*, 2005]), (2) the thermal and mechanical contraction of post-1968 lava fields (e.g., Etna [*Stevens et al.*, 2001a]), and (3) gravitationally driven creep (e.g., Mombacho [*van Wyk de Vries and Francis*, 1997]), possibly exacerbated by subedifice fault movement (as predicted by the models of *Lagmay et al.* [2000] and observed at Etna [*Lundgren et al.*, 2004]). In sections 3.1–3.4 we consider the plausibilities of each of these explanations with respect to our InSAR measurements and other independent observations from the literature.

3.1. Magmatic Deflation

[27] Magma withdrawal is typically modeled using a decreasing pressure source beneath the volcano.

Figure 4. (a) Map of cumulative displacement (cm) between the first and last acquisition dates used in time series (29 December 2005 to 25 April 2009). The locations of time series shown in Figures 4d–4f are marked. (b) Thickness of lavas emplaced between 1968 and 2004 [after *Wadge et al.*, 2006]. (c) Temporal distribution of interferograms used in analysis. (d) Cumulative displacement (cm) for a representative point high on Arenal's flanks. Uncertainties found from Monte Carlo inversion for the displacement at each acquisition date relative to the last are shown as error bars, while the uncertainty in cumulative displacement is shown in pale gray. (e) Cumulative displacement from farther down the flank, showing lower rate of slip than in Figure 4d. (f) Time series of cumulative displacement indicative of block-like motion, showing a significant change in slip rate at the start of 2008.

Point pressure source forward models [*Mogi*, 1958] were used to test the limits that the observed pattern and shape of deformation impose on source location (auxiliary material). The generally accepted model for Arenal's plumbing is of a magma chamber in the middle to lower crust, receiving a continuous flux of mantle material [*Reagan et al.*, 1987; *Streck et al.*, 2005]. Phase equilibria place the depth at which magma pools at ~12–14 km. Magmatic deflation at these depths would produce a broader, more symmetrical signal with a more diffuse fringe pattern than we observe [e.g., *Pritchard and Simons*, 2004]. For subedifice depths (2–14 km), the modeled deformation is longer wavelength than that observed and cannot match the observed fringe spacing unless a massive volume change ($>5 \times 10^8$ m³) is introduced. In order to match both fringe spacing and signal extent a Mogi source must be at depths shallower than ~1.2 km, well within the height of the edifice (1.7 km). Studies of the petrology [*Ryder et al.*, 2006] and shallow conduit seismicity [*Lesage et al.*, 2006] are both consistent with a near steady state open magmatic system with a deep source and show no evidence of magma storage within 1 km of the summit, as would be required to cause the observed deformation. The lack of evidence for the presence of any significant volume of magma stored in Arenal's edifice allow us to discount magmatic deflation as the cause of the deformation.

3.2. Lava Subsidence

[28] Lava subsidence is caused by a combination of thermoelastic contraction and the repacking of irregular clasts during cooling. While mechanical contraction is thought to be a function only of lava thickness and time for a compositionally uniform flow [*Stevens et al.*, 2001b], thermoelastic contraction rate is dependent on both lava thickness and distance from the edge of the lava body [*Peck*, 1978]. InSAR observations of lava contraction at Etna show subsidence ~10 years after emplacement [*Stevens et al.*, 2001a, 2001b], while at Okmok (Aleutian Islands), lava subsidence of ~1.5 cm/yr has been measured on a flow over 35 years old [*Lu et al.*, 2005]. We therefore expect some deformation due to lava contraction at Arenal, where lavas are 0–42 years old.

[29] Typically, lava subsidence is characterized by fringes that end at the edge of young flows and peak subsidence coinciding with the thickest point in the lava field [e.g., *Pritchard and Simons*, 2004; *Lu et al.*, 2005]. Given the limited coherence over Arenal, the information on the angle of deformation provided by the resolved components of motion gives the best evidence against thermal contraction as the primary cause of deformation. Maximum contraction of lava flows is expected to occur perpendicular to the lava surface, so that motion would be predominantly downward, with a small component of motion toward the volcano (i.e., eastward on the western flank), in contrast to the high rate of westward motion resolved from our interferometric data. Clast repacking could be expected to act in a downslope direction but is unlikely to account for such a high rate. The lower-magnitude near-vertical deformation observed at the base of Arenal's slopes (Figure 3e) could conceivably reflect lava contraction and compaction, but the direction and magnitude of the signal above this height, and especially at heights over 900 m suggests than another process is dominant. Although lava subsidence may well contribute to the deformation signal at Arenal it cannot be the primary mechanism.

3.3. Gravity-Driven Deformation

[30] Gravity-driven deformation ranges from rapid catastrophic edifice collapse at velocities of tens of m/s [*Ward and Day*, 2003] to gravitational spreading, which typically occurs at rates of millimeters per year [*Lundgren et al.*, 2004]. Studies of debris flow deposits [*Duffield et al.*, 1982] and volcano morphology [*Borgia et al.*, 2000] show that such processes are widespread, but observations of the active processes and measurements of rate are sparse. Both rapid and gradual deformation develop as a result of the need to accommodate the increase in weight and volume of a growing volcano. The spatial scale and speed of failure depends on the mechanical properties of the edifice and substrate, the volume and internal structure of the edifice and the presence of external stresses such as those caused by magma intrusion or an earthquake. Slow spreading has been suggested as a precursor to sector collapse at several volcanoes [*van Wyk de Vries and Francis*, 1997].

[31] The direction and shape of deformation at Arenal are matched well by other observations of gravity driven deformation (see references in Table 1). Similarly constant rates of motion have also been used to infer that deformation is being driven by a constant load [*Lundgren et al.*, 2004]. There is no obvious thrust feature to accommodate this motion at the base of the western slope, but such a feature may be obscured by the presence of drainage channels and rockfall debris. The rate of motion

Table 1. Summary of Measurements of Subaerial Gradual Volcano Spreading

Volcano	Inferred Deformation Mechanism	Measurement Type	Rate (cm/yr)	Key References
Etna	edifice fault movement	diff. InSAR extension	0.75	*Lundgren et al.* [2004]
Concepción	substrate flow	GPS	0–5 extension	*Borgia and van Wyk de Vries* [2003]
Colima	edifice compaction	precision leveling and GPS	<7 horizontal	*Murray and Wooller* [2002]
Vesuvius	substrate flow and faulting	diff. InSAR	0.6	*Borgia et al.* [2005]
Kilauea (subaerial)	basal decollement sliding	trilateration and tilt	6–10 (1983–2000)	*Delaney and Denlinger* [1999]
Arenal	edifice sliding	diff. InSAR	7	this work

of 7 cm/yr is high compared to other measurements of subaerial gravity-driven motion (Table 1), but within the very broad range of 1–50 cm/yr suggested by *van Wyk de Vries and Francis* [1997] for precursory spreading for flank collapse.

[32] Arenal shows several characteristics associated with shallower edifice failure at other volcanoes, including a layered structure and steep, conical morphology [*Voight*, 2000]. Its edifice is constructed from interbedded lavas and tephras, with heterogeneities in structure controlling the location of failure plane. Asymmetry predates Arenal's current phase of eruption, with thinner tephra deposits and longer lava flows on the eastern side [*Borgia et al.*, 1988]. Lavas emplaced since 1968 have also significantly altered the shape of Arenal's cone, increasing the load on the western sector of the volcano and the steepness of the slopes as crater C has become the summit. Lava effusion since 1968 has increased the volume of Arenal's edifice by 4%, with almost all of the new material being on its western side [*Wadge et al.*, 2006]. This pattern of emplacement is unusual among stratovolcanoes of similar size and composition and is a result of 40 years of near-continuous eruption.

[33] Although the motion of Arenal's western flank is best explained by a relatively shallow process, we cannot preclude the possibility that the Pliocene-Pleistocene volcanic deposits beneath the volcano are also deforming. Substrate deformation is used to explain some of the highest rates of gravity driven deformation observed at volcanoes (Table 1), especially where the substrate is weak. However, the ratio of brittle to ductile layer thickness beneath Arenal appears too high to facilitate basal spreading [*Merle and Borgia*, 1996]. The presence of the strike-slip Danta fault below Arenal may also contribute to instability in the edifice, although its rate of motion is not known with enough accuracy to constrain this.

[34] Possible failure planes are at the base of the post-1968 lavas or on the interface between lavas from crater A (pre-1973) and crater C (post-1973). The shape and extent of the youngest lava fields have been well constrained by comparison of DEMs from 6 dates between 1968 and 2004 [*Wadge et al.*, 2006], so that we can subtract lava thicknesses from the SRTM DEM (acquired in 2000) to find the approximate level of the pre-1968 surface. Since there was no DEM acquisition between the end of effusion from crater A and the start from crater C, the location of this boundary must be estimated (Figure 3f). The base of the 1968 lavas lies on a layer of tephra from the lateral blast eruption and a loose paleosol surface, giving a sharp contrast in competence. We consider this the most likely sliding plane for a slow slope failure. The total volume of material above this plane is $550 \pm 80 \times 10^6$ m³ [*Wadge et al.*, 2006], giving a mass of 1.3×10^{12} kg [after *Wadge*, 1983].

3.4. Implications

[35] At least 20 major edifice collapses have occurred in the last 500 years at volcanoes globally [*Voight*, 2000]. Sector collapse can be triggered by cryptodome or dike intrusion [*Elsworth and Voight*, 1995], destabilization caused by an earthquake [*Lagmay et al.*, 2000] or the inevitable result of long-term slow spreading and core weakening [*van Wyk de Vries and Francis*, 1997]. Although Arenal is significantly younger and smaller than other volcanoes that have experienced flank collapse, the unusually high rate of deformation (~7 cm/yr) suggests that the western flank already has an established plane of failure. A magmatic intrusion, as thought to be responsible for the 1968 blast eruption, or a high-magnitude earthquake as may be expected on the subduction zone beneath the Nicoya peninsula [*Protti et al.*, 1994], could conceivably trigger failure on the western flank of Arenal. Although the magma

chamber is believed to be in the middle to lower crust (section 3.1), it is possible that a collapse event could cause sudden decompression of a shallow conduit [*Manconi et al.*, 2009]. Arenal's shallow conduits experience a cycle of sealing, overpressurization and explosive rupture, with a correlation between volcanoseismic activity and Earth tides that implies strong sensitivity of the system to changes in confining pressure or stresses [*Williams-Jones*, 2001]. Even a small-scale gravitational failure has the potential to trigger an explosive eruption. The relatively constant rate of sliding indicates that Arenal's western flank has been in a steady state during the period of observation, but it is unclear whether this is stabilizing or destabilizing the slope. Any rapid increase in the rate of sliding may be taken as a precursor to collapse, so monitoring the deformation of Arenal's western slopes is important for detecting an increase in risk to the population around the volcano.

4. Conclusions

[36] We measured the deformation of Volcán Arenal, Costa Rica, using both ALOS and Radarsat interferograms between 2005 and 2009. The good spatial coverage and high resolution of the InSAR data allowed us to measure an unusual volcanic deformation signal that would have been unresolvable with fewer measurement points. This demonstrates InSAR's strength as a tool for observing and analyzing complex deformation systems. Arenal's lower western flanks, to which interferogram coherence is limited, are moving downslope at an angle of ~55° below the horizontal plane and a consistent average speed of about 7 cm/yr. The close fringe spacing and small spatial wavelength of deformation are indicative of a shallow source, which we attribute to slow gravity-driven slip. Our favored location for the sliding plane is the boundary between post-1968 eruption lavas and the paleosols and older eruptive products below, although it is conceivable that it is even shallower. The instability of Arenal's western slopes is a consequence of the volcano's asymmetric, composite structure and the rapid increase in loading of the western flank since 1968. Other reported observations of gravity-driven deformation are of significantly slower spreading caused by subedifice deformation, making Arenal unusual. Monitoring Arenal is vital for scientific and hazard purposes. Distinguishing between constant and discontinuous block-like motion and establishing depth to sliding plane(s) is important for understanding the deformation mechanism. Any increase

in the rate of sliding on Arenal's western flanks may also indicate potential collapse.

References

Alvarado, G. E., G. J. Soto, H. U. Schmincke, L. L. Bolge, and M. Sumita (2006), The 1968 andesitic lateral blast eruption at Arenal volcano, Costa Rica, *J. Volcanol. Geotherm. Res.*, *157*, 9–33, doi:10.1016/j.jvolgeores.2006.03.035.

Alvarado, G. E., S. Carboni, M. Cordero, M. Aviles, and M. Valverde (2010), Stability of the cone and the foundation of Arenal volcano, Costa Rica, paper presented at Cities on Volcanoes, Cabildo Insular de Tenerife, Tenerife, Canary Islands, 31 May to 4 June.

Berardino, P., G. Fornaro, R. Lanari, and E. Sansosti (2002), A new algorithm for surface deformation monitoring based on small baseline differential SAR interferograms, *IEEE Trans. Geosci. Remote Sens.*, *40*, 2375–2383, doi:10.1109/TGRS.2002.803792.

Biggs, J., D. P. Robinson, and T. H. Dixon (2009), The 2007 Pisco, Peru, earthquake (M8.0): Seismology and geodesy, *Geophys. J. Int.*, *176*, 657–669, doi:10.1111/j.1365-246X.2008.03990.x.

Borgia, A., and B. van Wyk de Vries (2003), The volcano-tectonic evolution of Concepción, Nicaragua, *Bull. Volcanol.*, *65*, 248–266, doi:10.1007/s00445-002-0256-8.

Borgia, A., C. Poore, M. J. Carr, W. G. Melson, and G. E. Alvarado (1988), Structural, stratigraphic, and petrologic aspects of the Arenal-Chato volcanic system, Costa Rica: Evolution of a young stratovolcanic complex, *Bull. Volcanol.*, *50*, 86–105, doi:10.1007/BF01275171.

Borgia, A., P. T. Delaney, and R. P. Denlinger (2000), Spreading volcanoes, *Annu. Rev. Earth Planet. Sci.*, *28*, 539–570, doi:10.1146/annurev.earth.28.1.539.

Borgia, A., et al. (2005), Volcanic spreading of Vesuvius, a new paradigm for interpreting its volcanic activity, *Geophys. Res. Lett.*, *32*, L03303, doi:10.1029/2004GL022155.

Chen, C. W., and H. A. Zebker (2002), Phase unwrapping for large SAR interferograms: Statistical segmentation and generalized network models, *IEEE Trans. Geosci. Remote Sens.*, *40*, 1709–1719, doi:10.1109/TGRS.2002.802453.

Delaney, P. T., and R. P. Denlinger (1999), Stabilization of volcanic flanks by dike intrusion: An example from Kilauea, *Bull. Volcanol.*, *61*, 356–362, doi:10.1007/s004450050278.

Duffield, W., L. Stieltjes, and J. Varet (1982), Huge landslide blocks in the growth of Piton de la Fournaise, La Réunion, and Kilauea volcano, Hawaii, *J. Volcanol. Geotherm. Res.*, *12*, 147–160, doi:10.1016/0377-0273(82)90009-9.

Elsworth, D., and B. Voight (1995), Dike intrusion as a trigger for large earthquakes and the failure of volcano flanks, *J. Geophys. Res.*, *100*, 6005–6024, doi:10.1029/94JB02884.

Fialko, Y., M. Simons, and D. Agnew (2001), The complete (3-D) surface displacement field in the epicentral area of the 1999 M_w 7.1 Hector Mine earthquake, California, from space geodetic observations, *Geophys. Res. Lett.*, *28*, 3063–3066, doi:10.1029/2001GL013174.

Fournier, T. J., M. E. Pritchard, and S. N. Riddick (2010), Duration, magnitude, and frequency of subaerial volcano deformation events: New results from Latin America using InSAR and a global synthesis, *Geochem. Geophys. Geosyst.*, *11*, Q01003, doi:10.1029/2009GC002558.

Hooper, A., H. Zebker, P. Segall, and B. Kampes (2004), A new method for measuring deformation on volcanoes and other natural terrains using InSAR persistent scatterers, *Geophys. Res. Lett.*, *31*, L23611, doi:10.1029/2004GL021737.

Lagmay, A. M. F., B. van Wyk de Vries, N. Kerle, and D. M. Pyle (2000), Volcano instability induced by strike-slip faulting, *Bull. Volcanol.*, *62*, 331–346, doi:10.1007/s004450000103.

Lesage, P., M. M. Mora, G. E. Alvarado, J. Pacheco, and J. P. Metaxan (2006), Complex behaviour and source model of the tremor at Arenal volcano, Costa Rica, *J. Volcanol. Geotherm. Res.*, *157*, 49–59, doi:10.1016/j.jvolgeores.2006.03.047.

Lu, Z., and J. T. Freymueller (1998), Synthetic aperture radar interferometry coherence analysis over Katmai volcano group, Alaska, *J. Geophys. Res.*, *103*, 29,887–29,894, doi:10.1029/1998JB02410.

Lu, Z., T. Masterlark, and D. Dzurisin (2005), Interferometric synthetic aperture radar study of Okmok volcano, Alaska, 1992–2003: Magma supply dynamics and postemplacement lava flow deformation, *J. Geophys. Res.*, *110*, B02403, doi:10.1029/2004JB003148.

Lundgren, P., F. Casu, M. Manzo, A. Pepe, P. Berardino, E. Sansosti, and R. Lanari (2004), Gravity and magma induced spreading of Mount Etna volcano revealed by satellite radar interferometry, *Geophys. Res. Lett.*, *31*, L04602, doi:10.1029/2003GL018736.

Manconi, A., M.-A. Longpre, T. R. Walter, V. R. Troll, and T. H. Hansteen (2009), The effects of flank collapses on volcano plumbing systems, *Geology*, *37*, 1099–1102, doi:10.1130/G30104A.1.

Merle, O., and A. Borgia (1996), Scaled experiments of volcanic spreading, *J. Geophys. Res.*, *101*, 13,805–13,818, doi:10.1029/95JB03736.

Minakami, T., and S. Utibori (1969), The 1968 eruption of volcano Arenal, Costa Rica, *Bull. Earthquake Res. Inst.*, *47*, 783–802.

Mogi, K. (1958), Relations between the eruptions of various volcanoes and the deformations of the ground surfaces around them, *Bull. Earthquake Res. Inst.*, *36*, 99–134.

Murray, L. K., and J. B. Wooller (2002), Persistent summit subsidence at Volcán de Colima, México, 1982–1999: Strong evidence against Mogi deflation, *J. Volcanol. Geotherm. Res.*, *117*, 69–78, doi:10.1016/S0377-0273(02)00236-6.

Peck, D. L. (1978), Cooling and vesiculation of Alae lava lake, Hawaii, *U.S. Geol. Surv. Prof. Pap.*, *935*.

Pritchard, M. E., and M. Simons (2004), An InSAR-based survey of volcanic deformation in the central Andes, *Geochem. Geophys. Geosyst.*, *5*, Q02002, doi:10.1029/2003GC000610.

Protti, M., F. Gündel, and K. McNally (1994), The geometry of the Wadati-Benioff zone under southern Central America and its tectonic significance: Results from a high-resolution local seismographic network, *Phys. Earth Planet. Inter.*, *84*, 271–287, doi:10.1016/0031-9201(94)90046-9.

Reagan, M. K., J. B. Gill, E. Malavassi, and M. O. Garcia (1987), Changes in magma composition at Arenal volcano, Costa Rica, 1968–1985: Real-time monitoring of open-system differentiation, *Bull. Volcanol.*, *49*, 415–434, doi:10.1007/BF01046634.

Rodriguez, E., C. S. Morris, and J. E. Belz (2006), A global assessment of the SRTM performance, *J. Am. Soc. Photogramm. Remote Sens.*, *72*, 249–260.

Rosen, P., A. Hensley, S. Gurrola, E. Rogez, F. Chan, S. Martin, and E. Rodriguez (2001), SRTM C-band topographic data: Quality assessments and calibration activities, *Int. Geosci. Remote Sens. Symp.*, *2*, 739–741.

Rosen, P. A., S. Hensley, G. Peltzer, and M. Simons (2004), Updated repeat orbit interferometry package released, *Eos Trans. AGU*, *85*(5), 47, doi:10.1029/2004EO050004.

Ryder, C. H., J. B. Gill, F. Tepley III, F. Ramos, and M. Reagan (2006), Closed to open system differentiation at Arenal volcano (1968–2003), *J. Volcanol. Geotherm. Res.*, *157*, 75–93, doi:10.1016/j.jvolgeores.2006.03.046.

Schmidt, D. A., and R. Bürgmann (2003), Time-dependent land uplift and subsidence in the Santa Clara valley, California, from a large interferometric synthetic aperture radar data set, *J. Geophys. Res.*, *108*(B9), 2416, doi:10.1029/2002JB002267.

Stevens, N. F., G. Wadge, and C. A. Williams (2001a), Post-emplacement lava subsidence and the accuracy of ERS InSAR digital elevation models of volcanoes, *Int. J. Remote Sens.*, *22*, 819–828, doi:10.1080/01431160051060246.

Stevens, N. F., G. Wadge, C. A. Williams, J. G. Morley, J. Muller, J. B. Murray, and M. Upton (2001b), Surface movements of emplaced lava flows measured by synthetic aperture radar interferometry, *J. Geophys. Res.*, *106*, 11,293–11,314, doi:10.1029/2000JB900425.

Streck, M. J., M. A. Dungan, F. Bussy, and E. Malavassi (2005), Mineral inventory of continuously erupting basaltic andesites at Arenal volcano, Costa Rica: Implications for interpreting monotonous, crystal-rich, mafic arc stratigraphies, *J. Volcanol. Geotherm. Res.*, *140*, 133–155, doi:10.1016/j.jvolgeores.2004.07.018.

van Wyk de Vries, B., and P. Francis (1997), Catastrophic collapse at stratovolcanoes induced by gradual volcano spreading, *Nature*, *387*, 387–390.

Voight, B. (2000), Structural stability of andesite volcanoes and lava domes, *Philos. Trans. R. Soc. London*, *A358*, 1663–1703.

Wadge, G. (1983), The magma budget of Volcan Arenal, Costa Rica from 1968 to 1980, *J. Volcanol. Geotherm. Res.*, *19*, 281–302, doi:10.1016/0377-0273(83)90115-4.

Wadge, G., et al. (2002), Atmospheric models, GPS and InSAR measurements of the tropospheric water vapour field

over Mount Etna, *Geophys. Res. Lett.*, *29*(19), 1905, doi:10.1029/2002GL015159.

Wadge, G., D. Oramas Dorta, and P. D. Cole (2006), The magma budget of Volcán Arenal, Costa Rica from 1980 to 2004, *J. Volcanol. Geotherm. Res.*, *157*, 60–74, doi:10.1016/j.jvolgeores.2006.03.037.

Ward, S. N., and S. Day (2003), Ritter Island Volcano-lateral collapse and the tsunami of 1888, *Geophys. J. Int.*, *154*, 891–902, doi:10.1046/j.1365-246X.2003.02016.x.

Williams-Jones, G. (2001), A model of degassing and seismicity at Arenal Volcano, Costa Rica, *J. Volcanol. Geotherm. Res.*, *108*, 121–139, doi:10.1016/S0377-0273(00)00281-X.

Wright, T. J., B. E. Parsons, and Z. Lu (2004), Toward mapping surface deformation in three dimensions using InSAR, *Geophys. Res. Lett.*, *31*, L01607, doi:10.1029/2003GL018827.

Zebker, H. A., F. Amelung, and S. Jonsson (2000), Remote sensing of volcano surface and internal processes using radar interferometry, in *Remote Sensing of Active Volcanism*, *Geophys. Monogr. Ser.*, vol. 116, edited by P. J. Mouginis-Mark, J. A. Crisp, and J. H. Fink, pp. 179–205, AGU, Washington, D. C.